



Critical polynomials in the nonplanar and continuum percolation models

Wenhui Xu ^{1,2}, Junfeng Wang,^{3,*} Hao Hu ^{1,†} and Youjin Deng^{2,4,‡}

¹*School of Physics and Materials Science, Anhui University, Hefei, Anhui 230601, China*

²*Hefei National Laboratory for Physical Sciences at the Microscale and Department of Modern Physics, University of Science and Technology of China, Hefei, Anhui 230026, China*

³*School of Electronic Science and Applied Physics, Hefei University of Technology, Hefei, Anhui 230009, China*

⁴*MinJiang Collaborative Center for Theoretical Physics, College of Physics and Electronic Information Engineering, Minjiang University, Fuzhou 350108, China*



(Received 21 October 2020; accepted 15 January 2021; published 12 February 2021)

Exact or precise thresholds have been intensively studied since the introduction of the percolation model. Recently, the critical polynomial $P_B(p, L)$ was introduced for planar-lattice percolation models, where p is the occupation probability and L is the linear system size. The solution of $P_B = 0$ can reproduce all known exact thresholds and leads to unprecedented estimates for thresholds of unsolved planar-lattice models. In two dimensions, assuming the universality of P_B , we use it to study a nonplanar lattice model, i.e., the equivalent-neighbor lattice bond percolation, and the continuum percolation of identical penetrable disks, by Monte Carlo simulations and finite-size scaling analysis. It is found that, in comparison with other quantities, P_B suffers much less from finite-size corrections. As a result, we obtain a series of high-precision thresholds $p_c(z)$ as a function of coordination number z for equivalent-neighbor percolation with z up to $O(10^5)$ and clearly confirm the asymptotic behavior $zp_c - 1 \sim 1/\sqrt{z}$ for $z \rightarrow \infty$. For the continuum percolation model, we surprisingly observe that the finite-size correction in P_B is unobservable within uncertainty $O(10^{-5})$ as long as $L \geq 3$. The estimated threshold number density of disks is $\rho_c = 1.436\,325\,05(10)$, slightly below the most recent result $\rho_c = 1.436\,325\,45(8)$ of Mertens and Moore obtained by other means. Our work suggests that the critical polynomial method can be a powerful tool for studying nonplanar and continuum systems in statistical mechanics.

DOI: [10.1103/PhysRevE.103.022127](https://doi.org/10.1103/PhysRevE.103.022127)

I. INTRODUCTION

Percolation theory [1] has been extensively studied for more than 60 years since it was first proposed by Broadbent and Hammersley [2]. It concerns the formation of connected components in random systems, and the percolation transition is one of the simplest examples of phase transitions. Despite the simplicity of its definition, the calculation of percolation thresholds is a very challenging problem. For the convenience of readers, we shall briefly recall some of the methods for analytically solving percolation thresholds in the past 60 years.

In the early years, only a few special classes of two-dimensional (2D) lattices could be exactly solved by using duality or matching properties of the lattices. For a given planar lattice \mathcal{L} , the dual lattice \mathcal{L}^* can be obtained by doing the following: (i) On each face of \mathcal{L} , place a vertex which serves as a vertex of \mathcal{L}^* ; (ii) for any two vertices of \mathcal{L}^* , add an edge between them if the corresponding two faces of \mathcal{L} have a common edge. For bond percolation, the thresholds of a lattice \mathcal{L} and its dual lattice \mathcal{L}^* are related by

$$p_c^{\text{bond}}(\mathcal{L}) + p_c^{\text{bond}}(\mathcal{L}^*) = 1. \quad (1)$$

Given a planar lattice \mathcal{L}_0 , a pair of matching lattices can be constructed by doing the following: (i) Select any subset of the faces of \mathcal{L}_0 , and fill in all the possible diagonals inside these faces to form a new graph \mathcal{L} ; (ii) select the faces that are not selected in step (1), and fill in all the possible diagonals in these faces to form another graph \mathcal{L}' . For site percolation, a similar relation between a pair of matching lattices \mathcal{L} and \mathcal{L}' is

$$p_c^{\text{site}}(\mathcal{L}) + p_c^{\text{site}}(\mathcal{L}') = 1. \quad (2)$$

From Eqs. (1) and (2), all bond percolation thresholds on the self-dual lattices and site percolation thresholds on the self-matching lattices are known to be $p_c = 1/2$. Examples include bond percolation on the square and martini-B lattice, and site percolation on the triangular, union jack, and asanoha [dual to the $(3, 12^2)$] lattice [3]. Typical examples of self-dual and self-matching lattices are shown in Fig. 1.

In 1964, Sykes and Essam [4] introduced into the percolation field the star-triangle transformation, which had been used for electrical circuits [5] as well as for the Ising model [6]. By use of the star-triangle transformation and bond-to-site transformation, they found the exact values of bond percolation thresholds on the triangular and honeycomb lattices, and of the site percolation threshold on the kagome lattice. The star-triangle transformation was further generalized for bond percolation on the bowtie lattice in 1984 [7] and

*wangjf@hfut.edu.cn

†huhao@ahu.edu.cn

‡yjdeng@ustc.edu.cn

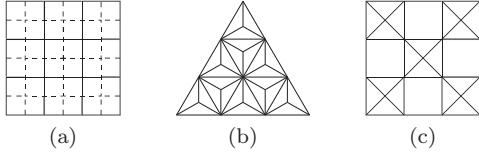


FIG. 1. (a) A typical example of a self-dual lattice. The square lattice (solid line) and its dual lattice (dash line) are topologically identical. (b) The asanoha lattice [dual to the $(3, 12^2)$ lattice]. It is self-matching since any 2D infinite lattice that is fully triangulated is a self-matching lattice. (c) The covering lattice of bond percolation on the square lattice. It is self-matching according to the argument in Ref. [4]. Here the diagonal bonds are nonplanar, and actually for all cases where the faces are not triangular, the matching lattice is always nonplanar.

site percolation on the martini lattice in 2006 [8]. Here we simply illustrate this method without proving it. As shown in Fig. 2(a), one replaces the bonds of every unit cell of the triangular lattice with a star, which transforms the triangular lattice into the honeycomb lattice. Supposing that the bonds of the two lattices are occupied with probabilities p and p^* , respectively, and that the corresponding percolation thresholds are p_c and p_c^* , one considers bond percolation on an individual “star-triangle” shown in Fig. 2(b). The probability of A being connected to both B and C , which is denoted as $P(A \rightarrow B, A \rightarrow C)$ on the triangular lattice and $P^*(A \rightarrow B, A \rightarrow C)$ on the honeycomb lattice, can be obtained as

$$P(A \rightarrow B, A \rightarrow C) = 3p^2 - 2p^3$$

and

$$P^*(A \rightarrow B, A \rightarrow C) = p^{*3}.$$

Following the argument in Ref. [4], the critical surface is defined as

$$P(A \rightarrow B, A \rightarrow C) = P^*(A \rightarrow B, A \rightarrow C). \quad (3)$$

Moreover, the duality between the triangular and honeycomb lattices guarantees that p_c and p_c^* are related by Eq. (1). Combining Eq. (1) and (3), one obtains

$$p_c^3 - 3p_c + 1 = 0. \quad (4)$$

Equation (4) has only one root at $p_c = 2 \sin \pi/18$ in the range $[0,1]$, which is exactly the bond percolation threshold of the triangular lattice. Besides Eq. (3), there are other connectivities that should be tested. For example, the probability of A being connected to B but not C , denoted as $P(A \rightarrow B, A \nrightarrow C)$

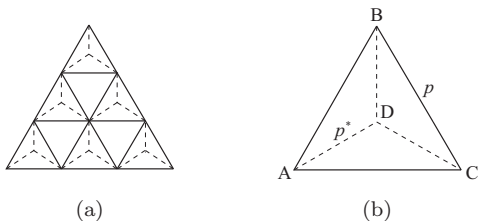


FIG. 2. (a) The star-triangle transformation on the triangular lattice; (b) one individual star-triangle with the bond probabilities p and p^* .

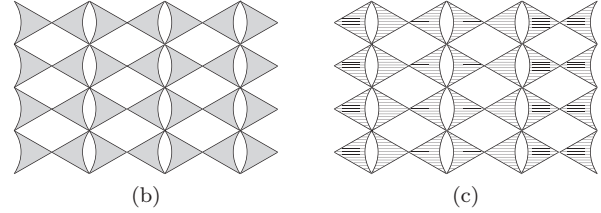
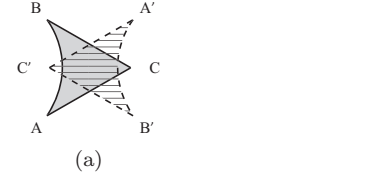


FIG. 3. The triangle-triangle transformation on a basic cell is shown in (a). The shaded region can contain any interactions among the vertices A, B, C . Panel (b) is an example of a self-dual lattice (the bowtie graph) since it is invariant under this triangle-triangle transformation, as shown in (c).

on the triangle lattice, is

$$P(A \rightarrow B, A \nrightarrow C) = p(1 - p)^2$$

and on the honeycomb lattice is

$$P^*(A \rightarrow B, A \nrightarrow C) = (1 - p^*)p^{*2}.$$

It is noted that $P(A \rightarrow B, A \nrightarrow C) = P^*(A \rightarrow B, A \nrightarrow C)$ leads to Eq. (1). Thus one cannot obtain an additional relation from the former equation, and it is similar for $(A \nrightarrow B, A \rightarrow C)$ and $(B \rightarrow C, B \nrightarrow A)$ cases. The condition $P(A \nrightarrow B, A \nrightarrow C) = P^*(A \nrightarrow B, A \nrightarrow C)$, however, is equivalent to Eq. (3). Generally speaking, the connectivity probabilities on both “star” and “triangle” are required to be equivalent at criticality.

In 2006, Scullard and Ziff [9,10] introduced the triangle-triangle transformation. This method extends the star-triangle transformation to lattices in which the basic cells do not necessarily lie in a triangular lattice, but in any self-dual arrangement. Here a “self-dual” lattice is defined as a lattice which is invariant under the triangle-triangle transformation, as shown in Fig. 3. The basic cell can represent any network of bonds and sites contained within the vertices A, B, C , as long as no sites are at these vertices. Similarly, they consider the connectivity between the vertices, which yields a general condition for criticality as

$$P_{\Delta}(A, B, C) = P_{\Delta}(\bar{A}, \bar{B}, \bar{C}), \quad (5)$$

where $P_{\Delta}(A, B, C)$ refers to the probability that three vertices A, B, C are connected, and $P_{\Delta}(\bar{A}, \bar{B}, \bar{C})$ refers to the probability that none are connected. Equation (5) leads to the threshold for any lattice that is self-dual under triangle-triangle transformation, and therefore significantly expands the number and types of lattices with exactly known thresholds [10,11]. For example, one can apply Eq. (5) to get bond percolation thresholds of the square, triangular, and honeycomb lattices. Other examples include site and bond percolation thresholds for the “martini,” “martini-A,” “martini-B,” and bowtie lattices [10,11]. The approach is also applied to determine the critical manifolds of inhomogeneous bond percolation on bowtie and checkerboard lattices [12], although for the latter and some

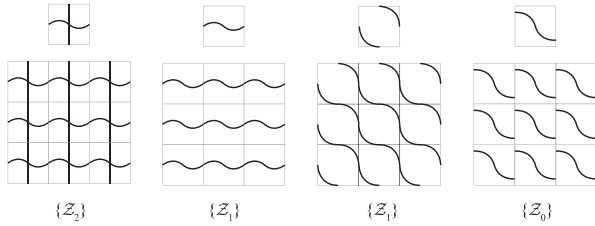


FIG. 4. Typical configurations on a 2D square with periodic boundary conditions. The number of different directions along which a configuration wraps decides its type among $\{Z_2\}$, $\{Z_1\}$, and $\{Z_0\}$.

cases of the former one needs to introduce artificial bonds with negative probability. It is noted that for the checkerboard case, the approach reproduces F. Y. Wu’s formula [13], which can be proven by the isoradial construction [12,14,15].

In the past few years, Scullard, Ziff, and Jacobsen developed the so-called critical polynomial method [16–25] which associates a graph polynomial with any 2D periodic lattice. This method originates from the observation that all the exact percolation thresholds appear as the roots of polynomials with integer coefficients. For example, the bond percolation threshold of the triangular lattice is the root of integer polynomial shown in Eq. (4). Scullard and Ziff first defined such a polynomial based on the linearity hypothesis and symmetries [16,17]. By employing a deletion-contraction algorithm, this polynomial can be applied on any 2D periodic lattice and provide, in principle, arbitrarily precise approximations for percolation thresholds [18,19]. Scullard and Jacobsen further gave an alternative probabilistic definition of the critical polynomial [20,21] which allows for much more efficient computations [22–25].

For simplicity, we describe the critical polynomial on a 2D square with periodic boundary conditions (a torus). All the configurations $\{C\}$ on the torus are classified into three types as $\{Z_0\}$, $\{Z_1\}$, and $\{Z_2\}$ according to their topological properties. As shown in Fig. 4, a configuration C belongs to $\{Z_2\}$ if it wraps along two different directions, to $\{Z_1\}$ if it wraps along one and only one direction, and to $\{Z_0\}$ if it does not wrap. Quantities R_2 , R_1 and R_0 represent the probabilities for a configuration to be in these classes respectively, i.e., the wrapping probabilities [26–28]. For planar lattices, when the configuration is of Z_2 -type (Z_0 -type), the corresponding configuration on the dual lattice is of Z_0 -type (Z_2 -type). This duality relation leads to $R_2 = R_0$ for self-dual lattices at critical point. Wrapping probabilities R_2 and R_0 are polynomial functions of the occupation probability p , and generally the critical polynomial is defined as $P_B \equiv R_2 - R_0$. From universality of R_2 and R_0 , the condition for criticality can be written as

$$P_B(p, L) = 0. \tag{6}$$

The properties of P_B on planar lattices are as follows:

- (i) The root of Eq. (6) provides an estimate for percolation the threshold p_c , and it satisfies $\lim_{L \rightarrow \infty} p(L) = p_c$.
- (ii) Finite-size correction vanishes for all solvable lattices: $P_B(p_c, L) = 0$. Therefore, the root of Eq. (6) gives the exact value of p_c for arbitrary system size L .

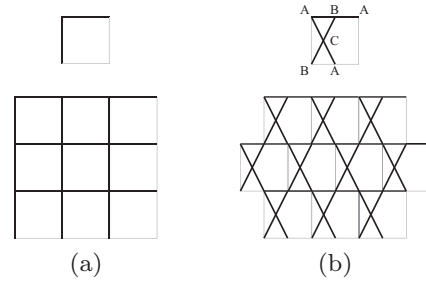


FIG. 5. (a) The basic cell of the square lattice with the bond probability p . (b) The basic cell of the kagome lattice with the site probability q .

(iii) $[p(L) - p_c] \simeq \sum_{k=1}^{\infty} A_k L^{-\Delta_k}$ vanishes rapidly for those lattices of which the p_c value is not exactly known. For unsolved Archimedean lattices, it is suggested empirically from transfer-matrix calculations that there are two different classes: one class has the first three scaling exponents as $\Delta_k = 4, 6, 8$ for $k = 1, 2, 3$, respectively; and the other class has $\Delta_k = 6, 7, 8$ for $k = 1, 2, 3$, respectively [25]. The first class includes the “Four-eight,” “Frieze,” “Cross,” “Snub square,” and “Ruby” lattices, and the other class includes the “Kagome,” “Three-twelve,” and “Snub hexagonal” lattices. But it remains unclear how to derive these values analytically and distinguish between the two classes [25].

Here we further explain these properties. For solvable lattices, the root of Eq. (6) in the range $[0,1]$ agrees with the exactly known thresholds regardless of the system size. A simple example is bond percolation on the square lattice. Considering the smallest repeated cell of the square lattice as shown in Fig. 5(a), and supposing each bond is occupied independently with probability p , the wrapping probabilities can be easily calculated as $R_2 = p^2$ and $R_0 = (1 - p)^2$, and therefore $P_B = p^2 - (1 - p)^2$. The only root of Eq. (6) is $p = 1/2$ which is exactly the bond percolation threshold of the square lattice. Another example is site percolation on the kagome lattice as shown in Fig. 5(b). The basic cell contains three vertices A, B, C that are independently occupied by sites with probability p , which is different from the cell in Fig. 3(a) for the triangle-triangle transformation where the vertices are not allowed to be occupied by sites. We calculate the wrapping probabilities as $R_2 = p^3$ and $R_0 = 3p(1 - p)^2 + (1 - p)^3$, which lead to $P_B = (1 - p)^3 - 3(1 - p) + 1$. Thus the site percolation threshold of the kagome lattice is given by the root of Eq. (6) as $p_c = 1 - 2 \sin \pi/18$, which is identical with the bond percolation threshold of the honeycomb lattice. This is a natural result because site percolation on the kagome lattice is isomorphic with bond percolation on the honeycomb lattice according to the bond-to-site transformation.

For unsolved lattices, we related the exponent Δ_1 to the leading correction exponent y_1 in the finite-size scaling of P_B as follows. In the renormalization formulation [29,30], as a dimensionless quantity, the finite-size scaling formula of P_B is

$$P_B(t, u_1, u_2, L) = P_B(L^{y_1} t, L^{y_1} u_1, L^{y_2} u_2), \tag{7}$$

where $t \propto p - p_c$ is the relevant thermal renormalization scaling field with the associated exponent $y_t = 1/\nu = 3/4 > 0$, and u_1, u_2 are two irrelevant fields with associated

exponents $y_2 < y_1 < 0$. With $P_B(p_c, L) = 0$ in the limit $L \rightarrow \infty$ and assuming $y_2 > 2y_1$, a first-order Taylor expansion of Eq. (7) gives $P_B(p, L) \simeq a_1(p - p_c)L^{y_1} + b_1L^{y_1} + b_2L^{y_2}$, where a_1 , b_1 and b_2 are nonuniversal constants. Substituting the expansion result into Eq. (6) leads to $p(L) - p_c = -(b_1/a_1)L^{y_1 - y_1} - (b_2/a_1)L^{y_2 - y_1}$. Thus the leading and sub-leading irrelevant exponents are given by $y_1 = y_i - \Delta_1$ and $y_2 = y_i - \Delta_2$, respectively. For unsolved Archimedean lattices, using the aforementioned empirically found Δ values, these tell that $y_1 = -3.25$ or -5.25 for P_B , which are much smaller than $y_1 = -2$ (expected as the subleading thermal renormalization exponent [31]) for conventional quantities such as wrapping probabilities [30].

Because of the above surprisingly small finite-size corrections, for many unsolved 2D periodic lattices, the critical polynomial method has been shown to be orders of magnitude more accurate in determining the percolation threshold than traditional techniques. It has also been applied to the q -state Potts model in the Fortuin-Kasteleyn representation to predict critical manifolds [21,22,24] with $P_B \equiv R_2 - qR_0$, where q is related to the symmetry of the model and $q \rightarrow 1$ corresponds to percolation. The generalization to nonplanar and continuum models, as far as we know, has not been reported yet. In these models, the value of P_B in the scaling limit is supposed to be zero as well due to universality, but the finite-size scaling (FSS) behavior is not clear. In particular, does the leading correction exponent belong to one of the two classes for Archimedean lattices?

The goal of this work is to explore the FSS behavior of P_B in nonplanar and continuum systems. For comparison purpose, FSS analysis is also performed for two wrapping probabilities R_0 , R_2 and a dimensionless ratio Q (defined later in Sec. II A) which is similar to the Binder ratio [32] extensively used in the study of phase transitions and critical phenomena. Extensive Monte Carlo (MC) simulations are conducted for a nonplanar lattice model, i.e., the 2D square-lattice bond percolation with many equivalent neighbors [30,33], and for the 2D continuum percolation with identical penetrable disks [34]. Periodic boundary conditions are employed as required for measuring P_B . The simulation results confirm that $P_B = 0$ for these two models at the critical point.

For the equivalent-neighbor percolation model, one of us (Y.D.) and collaborators [30,33] observed recently that as long as the coordination number z is finite, the model belongs to the short-range universality in two dimensions. The percolation threshold was determined by the critical polynomial, but the analysis details have not been reported. It is particularly informative to compare the finite-size correction in P_B and in more conventional quantities. In this work, the finite-size correction in P_B is found to be very small. For the model with $z = 8$ equivalent neighbors, the leading correction term of P_B scales as L^{y_1} with $y_1 \simeq -3$, while for R_0 , R_2 , and Q the leading correction term is $\sim L^{-2}$ or larger. The value -3 is close to $y_1 = -3.25$ for the first class of unsolved Archimedean lattices. For $z > 8$, two types of models are considered, which have different ways to involve neighbors, i.e., by coupling to all sites within a circle or a square. It is shown that the data of P_B are still consistent with the leading correction term being b_1L^{-3} . However, the amplitude b_1 cannot be well determined

by fitting the data, which indicates that our data are barely sufficient to detect the small finite-size correction. For very large z , e.g., $z \sim O(10^5)$, due to finite-size corrections, for sizes up to $L = 8192$, the crossing points of the wrapping probability deviate significantly from the percolation threshold, and the dimensionless ratio does not show a crossing at all in a wide range near p_c . Thus it is very hard to use the wrapping probability or the dimensionless ratio to determine precisely the percolation threshold for large z , as simulations for much larger L are needed. By fitting the FSS ansatz of P_B , it is possible to determine precisely values of zp_c for z up to $O(10^5)$ [33]. The data confirm the $z \rightarrow \infty$ asymptotic behavior $zp_c - 1 \simeq a_1z^{-1/2}$ for both types of models, and show that the coefficient a_1 takes different values for the two models. The latter indicates that $a_1z^{-1/2}$ represents a surface effect for the 2D model [35,36].

For the continuum model, it is found that at criticality the finite-size correction in P_B is too small to be observed for $L \geq 3$, i.e., $P_B(\rho_c, L) = 0$ almost holds for arbitrary L . This result is different from those of the unsolved Archimedean lattices and the equivalent-neighbor model, as well as exactly solved models for which $P_B(p_c, L) = 0$ exactly holds. In comparison, a leading correction term $\sim L^{-2}$ is confirmed for R_2 and $\sim L^{-1.5}$ for Q . Using P_B , the percolation threshold of the continuum model is determined as $\rho_c = 1.436\,325\,05(10)$, slightly below the most recent result $\rho_c = 1.436\,325\,45(8)$ given by Mertens and Moore [34].

The remainder of this work is organized as follows. Section II presents the simulation and results for the square-lattice bond percolation model with various number of equivalent neighbors, and Sec. III describes those for the 2D continuum percolation model. A brief discussion and conclusion is given in Sec. IV.

II. EQUIVALENT-NEIGHBOR PERCOLATION

A. Model and simulation

To the best of our knowledge, the equivalent neighbor model was first introduced by Dalton, Domb, and Sykes [37–39] to help bridge the gap in the understanding of spin systems between very short-range forces and very long-range forces. Recently, equivalent-neighbor percolation models were studied for bond percolation in 2D [30,33], 3D [40], and 4D [41], and for site percolation in 2D [42–45], 3D [45,46], and 4D [47]. In the square-lattice bond percolation model with equivalent neighbors, for each lattice site, there exists an edge between this site and any site within a given range. Two sites at the end of the same edge are called neighbors. Two ways to involve neighbors are considered: In type-1 model a site i with coordinates (x_i, y_i) is connected by an edge to all sites j satisfying $\sqrt{(x_i - x_j)^2 + (y_i - y_j)^2} \leq r$ (i.e., within a circle of radius r), and in type-2 model to all sites j satisfying both $|x_i - x_j| \leq r$ and $|y_i - y_j| \leq r$ (i.e., within a square of side length $2r$). As in the nearest-neighbor percolation, the equivalent-neighbor percolation is introduced by placing independently a bond on each edge with the same probability p .

We simulate the above models with periodic boundary conditions. Since there are many equivalent neighbors, the

TABLE I. Fit results of observables P_B , R_2 , R_0 , and Q for bond percolation on the square lattice with $z = 8$ equivalent neighbors. Entries “—” indicate that the corresponding parameters are set to be zero, and the numbers without error bars are fixed in the fits.

Obs.	L_{\min}	χ^2/DOF	y_t	p_c	O_0	q_1	b_1	y_1	b_2	y_2
P_B	8	25.8/32	0.84(9)	0.250 368 50(7)	0.000 008(5)	-2.7(8)	-0.17(2)	-2.98(7)	—	—
	9	23.8/27	0.82(9)	0.250 368 50(8)	0.000 007(6)	-3(1)	-0.18(4)	-3.0(1)	—	—
	5	34.0/38	0.84(8)	0.250 368 50(7)	0.000 007(5)	-2.7(8)	-0.34(10)	-3.19(10)	0.5(2)	-4
	6	31.4/37	0.84(8)	0.250 368 46(7)	0.000 004(5)	-2.7(8)	-0.30(9)	-3.2(2)	1.5(6)	-5
	6	30.8/37	0.84(8)	0.250 368 46(7)	0.000 004(5)	-2.7(8)	-0.24(5)	-3.12(10)	5(2)	-6
	8	30.6/34	3/4	0.250 368 40(2)	0	-3.6(2)	-0.21(2)	-3.08(4)	—	—
	9	26.4/29	3/4	0.250 368 40(2)	0	-3.7(2)	-0.23(3)	-3.14(6)	—	—
	10	29.8/29	3/4	0.250 368 39(2)	0	-3.7(2)	-0.169(2)	-3	—	—
	12	24.0/24	3/4	0.250 368 39(2)	0	-3.7(2)	-0.165(3)	-3	—	—
	14	10.6/17	3/4	0.250 368 5(5)	0.309 52(3)	-1.8(2)	0.032(5)	-1.56(7)	—	—
R_2	6	38.7/38	3/4	0.250 368 0(3)	0.309 50(1)	-1.7(1)	0.044(3)	-1.63(3)	-0.176(9)	-3
	8	28.4/32	3/4	0.250 368 2(3)	0.309 51(2)	-1.73(10)	0.034(3)	-1.57(4)	-0.75(8)	-4
	7	29.8/34	3/4	0.250 368 47(4)	0.309 526 275	-1.7(1)	0.055(2)	-1.72(1)	-0.219(8)	-3
	8	30.0/33	3/4	0.250 368 56(5)	0.309 526 275	-1.7(1)	0.038(1)	-1.62(1)	-0.84(4)	-4
R_0	10	22.2/27	3/4	0.250 369 1(2)	0.309 49(1)	2.0(1)	0.044(2)	-1.63(2)	—	—
	7	25.4/33	3/4	0.250 368 9(3)	0.309 50(2)	1.9(1)	0.049(5)	-1.67(4)	-0.03(2)	-3
	7	25.4/33	3/4	0.250 369 0(3)	0.309 49(1)	1.9(1)	0.046(3)	-1.65(3)	-0.08(5)	-4
	5	36.0/40	3/4	0.250 368 45(3)	0.309 526 275	1.9(1)	0.0632(9)	-1.768(5)	-0.079(3)	-3
	6	37.3/39	3/4	0.250 368 38(3)	0.309 526 275	1.9(1)	0.0529(7)	-1.715(7)	-0.20(2)	-4
Q	20	5.5/11	3/4	0.250 368(2)	0.960 17(2)	-0.28(2)	-0.034(4)	-1.58(5)	—	—
	12	18.9/21	3/4	0.250 369(1)	0.960 170(9)	-0.28(2)	-0.050(7)	-1.68(5)	0.24(4)	-3
	14	13.5/16	3/4	0.250 369(1)	0.960 17(1)	-0.27(2)	-0.038(5)	-1.61(5)	1.4(3)	-4

simulation would be time consuming if the edges are individually checked to be occupied or not. We apply an algorithm [33,48] which requires computer time that is almost independent of the number of neighbors z . The cluster wrapping is detected by a method [49,50] originally employed in simulations of Potts models. Quantities are sampled after all the clusters are constructed and a configuration is formed. From the sampled configurations, the following observables are calculated:

- (i) Wrapping probabilities R_0, R_1, R_2 , and the critical polynomial P_B .
- (ii) The dimensionless ratio $Q = \langle C_1 \rangle^2 / \langle C_1^2 \rangle$, where C_1 is the size of the largest cluster and $\langle \cdot \rangle$ means the statistical average.

At percolation threshold, clusters become fractal and the distribution of cluster sizes obeys some scaling-invariant form. A conventional method to locate the percolation threshold is then to utilize the scaling behavior of the cluster sizes. In particular, dimensionless ratios like the quantity Q are found very powerful because of their simple scaling form, and have a long history of being used in the study of critical phenomena [32,51]. The ratio Q , the wrapping probabilities and the critical polynomial P_B exhibit similar finite-size scaling behavior. When they are plotted versus the occupation probability, the crossings of the curves for different system sizes asymptotically converge to the percolation threshold and the critical values of these quantities are universal.

Simulations were first performed for the model with $z = 8$ neighbors. The type of the model is not specified, since the type-1 model shares the same 8 neighbors with the type-2 model. The system sizes in simulations range from $L = 4$ to

64, and the number of samples for each size at a given p is around 10^{10} to 10^{11} . Simulations were also conducted for several values of z from 148 ($r = 7$) to 50 616 ($r = 127$) for the type-1 model, and from 120 ($r = 5$) to 65 024 ($r = 127$) for the type-2 model. The system sizes for these models of $z > 8$ range from $L = 16$ to 8192.

B. Numerical results

The data of P_B are fitted by the least-square criterion using the following ansatz

$$O(p, L) = O_0 + q_1(p_c - p)L^{y_t} + b_1L^{y_1} + b_2L^{y_2}, \quad (8)$$

where $y_t = 1/\nu$ is the thermal renormalization exponent, and y_1, y_2 are the leading and subleading correction exponents, respectively. The second-order term $q_2(p_c - p)^2L^{2y_t}$ is not present due to duality [52], and effects of crossing scaling terms such as $c_1(p_c - p)L^{y_t+y_1}$ is found to be negligible. As a precaution against high-order correction terms that are not included in Eq. (8), we gradually exclude the data points for $L \leq L_{\min}$ and see how the residual χ^2 changes with respect to L_{\min} . Generally the fit result is satisfactory if the value of χ^2 is less than or close to the number of degrees of freedom (DOF) and the drop of χ^2 caused by increasing L_{\min} is no more than one unit per degree of freedom.

For $z = 8$, the fit results are summarized in Table I. If letting all parameters in Eq. (8) be free, the fitting procedure does not work, which indicates that our MC data are not sufficient to determine all parameters simultaneously. Therefore, we perform fits with some parameters being fixed. When setting $b_2 = 0$, the fit results show that the leading correction

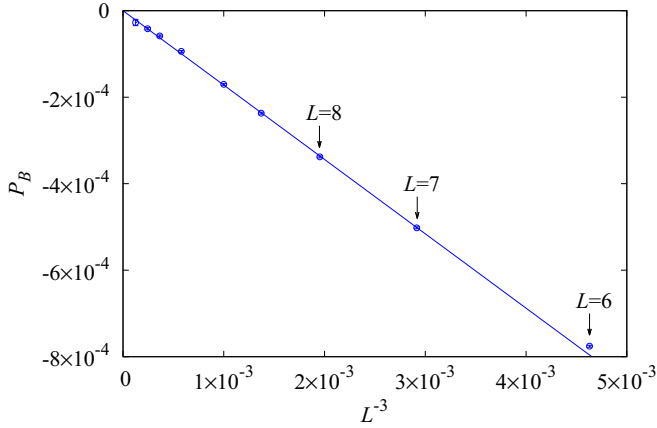


FIG. 6. P_B versus L^{-3} for bond percolation on a periodic square lattice with $z = 8$ equivalent neighbors, at $p = 0.250\,368\,385$ which is within the error margin of the estimate $p_c = 0.250\,368\,40(4)$. The solid line is a straight line with slope $b_1 \simeq -0.17$ obtained by fitting the data. From right (small) to left (large), sizes for other data points are $L = 9, 10, 12, 14, 16, 20$, respectively.

exponent is $y_1 \simeq -3$. In order to confirm this observation, we also perform the fits with y_2 being fixed at $-4, -5$, or -6 , but b_2 being free. And the results are consistent with $y_1 \simeq -3$. From these fits we also estimate $y_t = 0.84(11)$ and $P_{B0} = 0.000\,007(8)$, which are consistent with $y_t = 3/4$ [31] and $P_{B0} = 0$, as expected from universality of 2D ordinary percolation. We further perform the fits with both $y_t = 3/4$ and $P_{B0} = 0$ being fixed, which is helpful to give an accurate estimate of p_c .

Thus, from all fits with y_1 free, we estimate the leading correction exponent of P_B to be $y_1 = -3.0(3)$. And from all fits with P_B fixed at zero, we report our estimate of the percolation threshold as $p_c = 0.250\,368\,40(4)$. In Fig. 6, we plot P_B versus L^{-3} for our MC data at $p = 0.250\,368\,385$, which is within the error bar of our estimate of p_c . According to Eq. (8), at p_c and for large system sizes, P_B versus L^{y_1} should display approximately a straight line. This phenomenon is indeed observed in Fig. 6, which demonstrates our estimate of $y_1 \simeq -3$. The value -3 is close to $y_1 = y_t - \Delta_1 = -3.25$ for the first class of unsolved Archimedean lattices mentioned in the introduction. It is also noted that the magnitude of P_B is only in order $O(10^{-4})$, illustrating the smallness of finite-size corrections in P_B .

We also perform fits for R_0, R_2 , and Q by Eq. (8), and the results are also summarized in Table I. These lead to estimates of the leading correction exponent $y_1 \simeq -1.6$. The data could also be fitted by formulas with more sophisticated finite-size scaling, e.g., with second-order term $q_2(p_c - p)^2 L^{2y_t}$, and with leading correction terms proportional to L^{-2} and $\ln(L)L^{-2}$ for R_2 , and for Q with a correction term $\sim L^{-43/24}$ in addition to the latter two terms [30]. The results of universal quantities are well consistent with the exact result $R_{0,0} = R_{2,0} = 0.309\,526\,275$ [27,50] and with the previous estimate $Q_0 = 0.960\,17(1)$ [53]. From the estimate of the correction exponent y_1 , it is seen that the finite-size corrections for P_B decay more rapidly than those for R_0, R_2 , and Q .

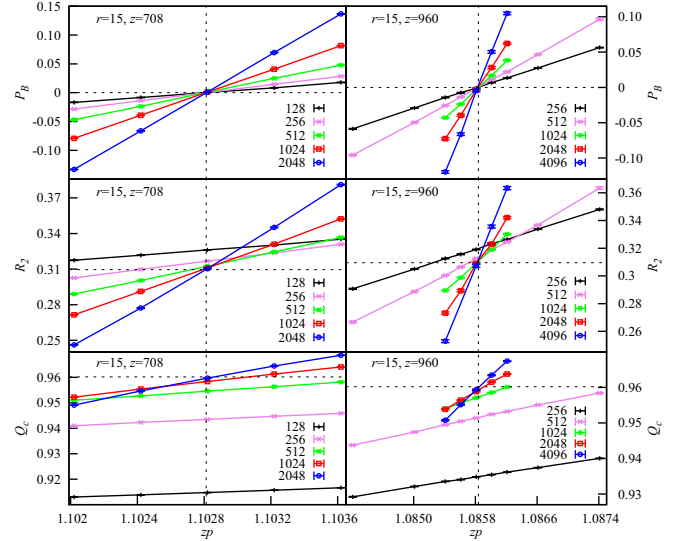


FIG. 7. Plots of P_B, R_2 , and Q versus zp for different system sizes L , for equivalent-neighbor percolation models with $r = 15$, corresponding to $z = 708$ and $z = 960$ for type-1 (left panel) and type-2 (right panel) models, respectively. Vertical dashed lines show the thresholds $zp_c = 1.102\,812(3)$ and $zp_c = 1.085\,839(5)$ [33] for type-1 and type-2 models, respectively. Horizontal dashed lines indicate the universal values of these quantities at criticality. The error bars of the data are smaller than the size of the data points. Values of L are given in the legend. The solid lines connecting data points are added for clarity.

For models with $z > 8$, we make plots for P_B , and compare them with those for other dimensionless quantities R_2 and Q . Figures 7 and 8 show the results for $r = 15$ and 127, corresponding to $z \sim O(10^3)$ and $O(10^5)$, respectively. We have the following observations. Firstly, curves for different sizes L cross well near the point $(zp_c, 0)$ for P_B , even for small relative sizes down to $L/(r+1) = 8$. Second, for R_2 , as L increases, the crossing points converge much slower than for P_B . For $r = 127$, the convergence is so slow that even the crossing point of curves for the largest two sizes deviates significantly from the critical point, and if not knowing the exact value of R_2 , a biased estimate of the critical point may be obtained. Finally, for Q , the crossing point of the largest two sizes is significantly different from (zp_c, Q_0) when $r = 15$, and the curves do not intersect at all near p_c when $r = 127$.

Fits are also performed for models with $z > 8$ using Eq. (8). For P_B , the leading correction exponent y_1 cannot be well determined when it is set as a parameter to be fitted. With fixed $y_1 = -3$, stable fit results can be obtained, though the resulting estimate of b_1 has a large error bar that is comparable to its absolute value. These tell that our data are barely sufficient to detect the small finite-size correction in P_B . The fit results also suggest that the second-order term $q_2(p_c - p)^2 L^{2y_t}$ is absent in the scaling of P_B . When fitting the data of R_2 and Q , the second-order term needs to be included. For R_2 at $r = 127$, if $R_{2,0}$ is not fixed in the fits, the estimate of p_c is significantly different from that obtained by fitting P_B , which confirms our second observation in last paragraph. For Q at $r = 127$, if Q_0 is not fixed, the estimate of p_c is also biased, and the estimate of Q_0 is different from the universal

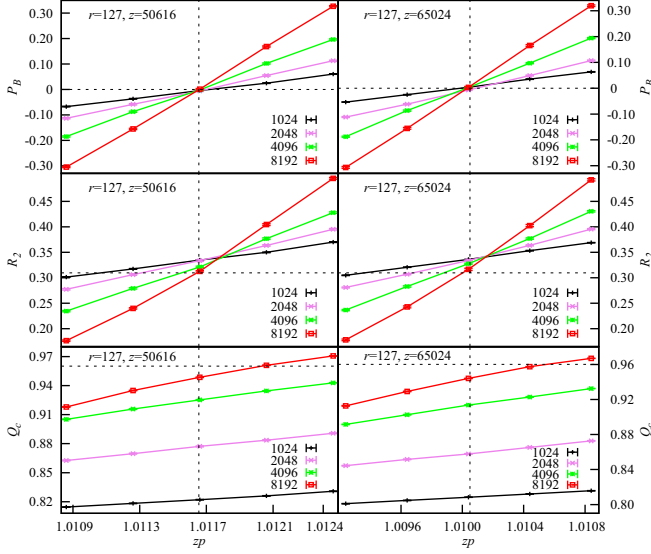


FIG. 8. Plots of P_B , R_2 , and Q versus zp for different system sizes L , for equivalent-neighbor percolation models with $r = 127$, corresponding to $z = 50\,616$ and $z = 65\,024$ for type-1 (left panel) and type-2 (right panel) models, respectively. Vertical dashed lines show the thresholds $zp_c = 1.011\,655(20)$ and $zp_c = 1.010\,05(3)$ [33] for type-1 and type-2 models, respectively. Horizontal dashed lines indicate the universal values of these quantities at criticality. The error bars of the data are smaller than the size of the data points. Values of L are given in the legend. The solid lines connecting data points are added for clarity.

value $0.960\,17(1)$; if Q_0 is fixed at the universal value, then one cannot get stable fit results, due to large and complicated finite-size corrections. Thus Q is not suitable for determining p_c when r (or equivalently z) is large, which is consistent with the previous observation for Q that at $r = 127$ curves for different sizes do not intersect near p_c .

The above results demonstrate that P_B also has much smaller finite-size corrections than other quantities when z is greater than 8. And this advantage of P_B becomes more obvious as z increases. Thus we use P_B to determine precisely percolation thresholds for various values of z for both type-1 and type-2 models. The results are summarized in Table II. From the table, it can be seen that, when z is large (e.g., $z > 100$), the value of zp_c decreases as z becomes larger, and it tends to approach the mean-field value $zp_c = z/(z-1)$ which equals to one in the limit $z \rightarrow \infty$. Using these estimates of zp_c , we plot $(zp_c - 1)z^{1/2}$ versus $z^{-1/2}$ for both types of models in Fig. 9. The intercept of the lines in the figure gives the value of a_1 , which is different for type-1 and type-2 models. The straight lines indicate that both models can be described by a correction term $a_2z^{-1/2}$ when z is large. Overall, the figure confirms that the threshold p_c satisfies $zp_c - 1 = a_1z^{-1/2}(1 + a_2z^{-1/2})$ when z is large [30,33].

For the asymptotic behavior of zp_c as $z \rightarrow \infty$, it has been conjectured that $zp_c - 1 \sim 1/r^{d-1}$ for 2D and 3D models [35,36], where d is the spatial dimension. Since $z \sim r^d$, this leads to $zp_c - 1 \sim 1/z^{(d-1)/d}$ for 2D and 3D models. When $d = 2$, it yields $zp_c - 1 \simeq a_1z^{-1/2}$ for large z , which is supported by our results above. Since r^{d-1} is proportional to the

TABLE II. Percolation threshold zp_c for the equivalent-neighbor percolation models of type-1 and type-2, with various number of neighbors z . Results for $z > 8$ have been reported in Ref. [33], for which one of us (Y.D.) is a coauthor.

Type-1		Type-2		
r	z	zp_c	z	zp_c
1	4	2	8	2.002 947 2(32)
$\sqrt{2}$	8	2.002 947 2(32)		
5			120	1.257 695(7) [33]
7	148	1.234 704(2) [33]	224	1.184 443(5) [33]
15	708	1.102 812(3) [33]	960	1.085 839(5) [33]
23	1652	1.066 297(7) [33]	2208	1.055 830(10) [33]
31	3000	1.048 803(8) [33]	3968	1.041 349(7) [33]
35.8	4016	1.042 043(5) [33]		
47	6920	1.031 871(16) [33]	9024	1.027 217(15) [33]
63	12452	1.023 640(20) [33]	16128	1.020 270(15) [33]
127	50616	1.011 655(20) [33]	65024	1.010 05(3) [33]

surface length or area, the asymptotic behavior of the form $a_1z^{-1/2}$ can be regarded as a surface effect for the 2D model. Our observation that a_1 is different for the two types of models also implies this surface effect, since the surfaces are different for type-1 and type-2 models.

III. CONTINUUM PERCOLATION

A. Model and simulation

Continuum percolation has been used to discuss the physical properties of complex fluids and disordered systems. The 2D continuum percolation with overlapping disks is particularly important because it corresponds to the randomly deposited networks of nanoparticles [54], which have various interesting properties and applications. In the 2D continuum percolation, a number (n) of randomly centered disks are distributed on a $L \times L$ square. The number n satisfies a Poisson distribution

$$P(n) = \frac{\lambda^n e^{-\lambda}}{n!}, \quad (9)$$

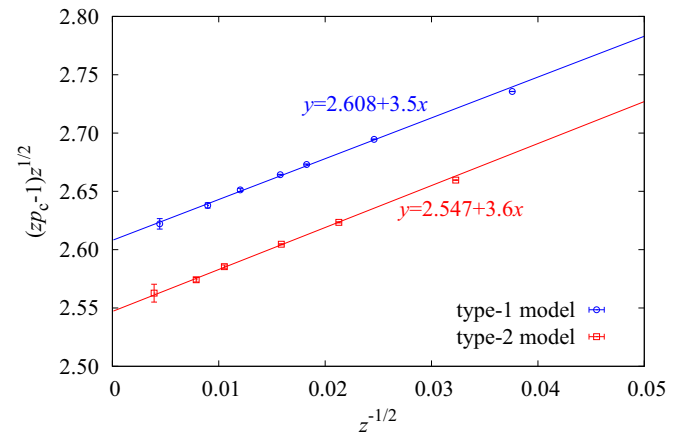


FIG. 9. Plot of $(zp_c - 1)z^{1/2}$ versus $z^{-1/2}$ for equivalent-neighbor models. The straight lines are obtained by fitting the data.

where $P(n)$ refers to the probability that n disks are distributed, and $\lambda = \rho L^2$ with ρ being the mean density. Two penetrable disks are connected if they overlap, and the n disks form connected groups with complex geometries. Various numerical studies have shown that continuum percolation with overlapping disks shares the same critical exponents with lattice percolation, indicating that they belong to the same universality class [55–57].

We simulate the continuum percolation model on a $L \times L$ square with periodic boundary conditions. The identical penetrable disks are of diameter one. In each trial, the number of objects n is determined by a random number generator following a Poisson distribution with mean density parameter ρ . The disks are randomly placed into the square using a uniform distribution. The cell-list method [58] is employed for efficiently finding neighboring disks. The same set of quantities as for the equivalent-neighbor model are sampled after all the clusters are constructed.

As in site percolation, any pair of overlapping disks in continuum percolation can be considered to be effectively connected by a bond between their centers. One then obtains a nonplanar graph by drawing all such bonds between pairs of overlapping disks. However, for any pair of crossing bonds, the disks at their ends must belong to the same cluster. This is similar to site percolation on the square lattice with nearest- and next-nearest-neighbor interactions (coordination number $z = 8$), for which four occupied sites on a square face, having a pair of diagonal bonds, must be in the same cluster. In other words, continuum percolation is like site percolation with compact neighborhoods where crossing connectivity cannot occur without simultaneously there being the presence of nearest-neighbor connectivity. Actually the latter can be mapped to problems of lattice percolation of extended shapes (e.g., disks), whose thresholds can be related to the continuum thresholds for objects of those shapes [45]. As a consequence, an interesting property arises for continuum percolation in 2D: The percolation of clusters and the void percolation of the unoccupied space are matching and if one percolates, then the other does not and vice versa.

A recent numerical study of the continuum percolation of identical penetrable disks was published by Mertens and Moore in 2012 [34]. In their work, wrapping probabilities were applied as observables, and an adaption of the Newman-Ziff algorithm was used for simulations [34,50]. They conducted extensive MC simulations for 50 different system sizes ranging from $L = 8$ to 2048, with sample sizes being 10^{10} for $L \leq 100$, 10^9 for $100 < L \leq 500$, and 10^6 for $500 < L \leq 2048$. In our work, we simulated 12 different sizes ranging from $L = 3$ to 512. The number of samples is about 10^{10} for $L \leq 100$ and 5×10^9 for $100 \leq L \leq 512$. It is noted that, though not used in this work, a similar Newman-Ziff approach as in Ref. [34] can also be used to calculate P_B as function of ρ , which might save some computer time since separate runs at different values of ρ are not needed.

B. Numerical results

Figure 10 shows the plots of quantities P_B , R_2 , and Q as a function of ρ for different L . From the plot of P_B , it can be

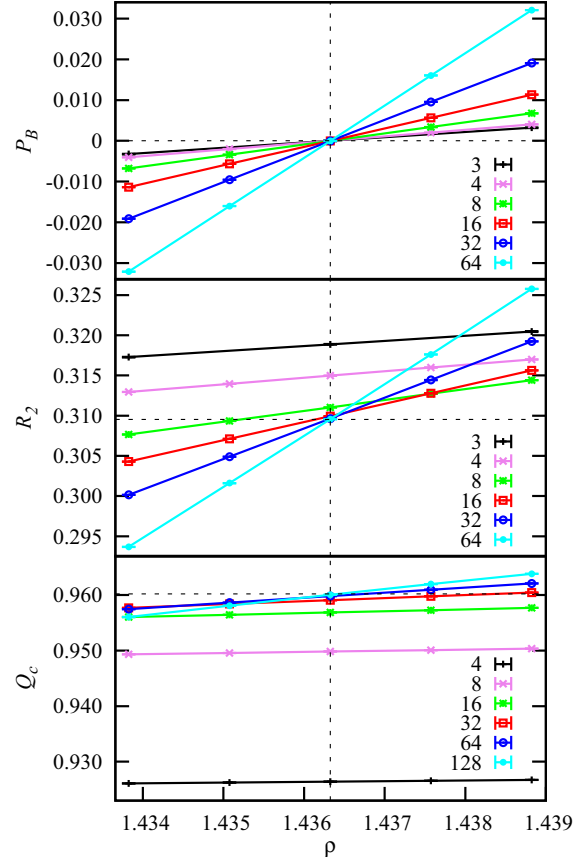


FIG. 10. Plots of P_B , R_2 , and Q versus ρ for different system sizes L for the continuum percolation model. Values of L are given in the legend. Vertical dashed line shows the threshold $\rho_c = 1.436325(10)$, and horizontal dashed lines indicate the universal values of these quantities at criticality. The error bars of the data are smaller than the size of the data points. The solid lines connecting data points are added for clarity.

seen that the curves cross very well near $\rho \simeq 1.4363$, which is a rough approximation for the percolation threshold with an uncertainty at the fourth decimal place. At criticality, the value of P_B is consistent with zero as expected from universality. For plots of R_2 and Q , when L is small, the curves cross at different points due to finite-size corrections. As L becomes larger, the intersections of curves converge to the critical point, with $R_{2,0} \simeq 0.309$ and $Q_0 \simeq 0.960$ being consistent with their universal values $R_{2,0} = 0.30952628$ [27,50] and $Q_0 = 0.96017(1)$ [53].

To examine the FSS behavior of sampled quantities, we fit the data by the ansatz

$$O(\rho, L) = O_0 + a_1(\rho_c - \rho)L^{y_1} + a_2(\rho_c - \rho)^2L^{2y_1} + b_1L^{y_1} + b_2L^{2y_1} + c_1(\rho_c - \rho)L^{y_1+y_1}, \quad (10)$$

where the thermal renormalization exponent is fixed at $y_1 = 3/4$. For P_B and wrapping probabilities, the leading correction exponent y_1 is fixed as the subleading thermal renormalization exponent -2 [31], which is supported by previous data of wrapping probabilities for 2D continuum percolation [34]. The fit results are shown in Table III.

TABLE III. Fit results of sampled quantities for the continuum percolation model. ‘‘Obs.’’ is the abbreviation of ‘‘observables.’’ Entries ‘‘—’’ indicate that the corresponding parameters are set to be zero, and the numbers without error bars are fixed in the fits.

Obs.	L_{\min}	χ^2/DOF	O_0	ρ_c	a_1	a_2	b_1	b_2	c_1	y_1
P_B	3	95.3/102	-0.000 002(1)	1.436 324 94(7)	-0.567 3(2)	0.001(3)				
	4	95.3/99	-0.000 002(1)	1.436 324 94(7)	-0.567 3(2)	0.001(3)				
	8	88.2/94	-0.000 003(2)	1.436 324 89(7)	-0.567 3(2)	0.001(3)				
	3	100.5/103	0	1.436 325 05(5)	-0.567 3(2)	0.001(2)				
	4	100.4/100	0	1.436 325 05(5)	-0.567 3(2)	0.001(2)	—	—	—	—
	8	98.4/95	0	1.436 325 05(5)	-0.567 3(2)	0.001(2)				
	3	100.7/104	0	1.436 325 05(5)	-0.567 3(2)	0				
	4	100.6/101	0	1.436 325 05(5)	-0.567 3(2)	0				
R_2	8	98.6/96	0	1.436 325 05(5)	-0.567 3(2)	0				
	16	72.0/69	0.309 526 275	1.436 324 88(7)	-0.283 6(2)	0.052(2)	0.118(2)	-2.9(3)	-0.02(4)	-2
	24	44.5/56	0.309 526 275	1.436 324 92(7)	-0.283 4(2)	0.052(2)	0.123(3)	-7(2)	-0.2(3)	-2
	32	37.3/51	0.309 526 275	1.436 324 97(8)	-0.283 5(2)	0.052(2)	0.131(7)	-16(7)	-0.3(3)	-2
R_0	16	65.2/69	0.309 526 275	1.436 324 95(7)	0.283 5(1)	0.056(2)	0.125(1)	-4.5(3)	0.04(4)	-2
	24	37.5/56	0.309 526 275	1.436 324 92(7)	0.283 2(2)	0.056(2)	0.129(3)	-8(2)	0.6(2)	-2
	32	36.3/51	0.309 526 275	1.436 324 91(8)	0.283 2(2)	0.056(2)	0.131(7)	-9(7)	0.6(2)	-2
	64	34.2/33	0.960 173(4)	1.436 327(1)	-0.040 89(3)	0.014 5(1)	-0.20(2)		-0.04(2)	-1.51(2)
Q	96	19.3/24	0.960 176(7)	1.436 327(2)	-0.040 87(4)	0.014 5(2)	-0.18(4)	—	-0.08(7)	-1.48(5)
	128	14.4/20	0.960 2(1)	1.436 337(8)	-0.040 83(6)	0.014 5(2)	-0.03(3)		-0.01(1)	-1.0(3)

For P_B , the amplitudes b_1 , b_2 , and c_1 are found to be consistent with zero when they are set as parameters to be fitted, which indicates that the finite-size correction is very small. The presented results for P_B are from fits with b_1 , b_2 , and c_1 being fixed at zero. When O_0 is a free fit parameter, the fitted values of O_0 for P_B is consistent with zero within one error bar, as expected from the universality of P_B . Then fits are performed with fixed $O_0 = 0$. It is found that, with only the second and third terms, Eq. (10) can well describe the P_B data for $L \geq 3$ near the critical point, yielding a stable estimate of ρ_c as 1.436 325 05(5). Moreover, the fit results have a_2 being consistent with zero, which implies that the second-order term $a_2(\rho_c - \rho)^2 L^{3/2}$ vanishes also due to duality [52]. Fits with fixed $a_2 = 0$ also lead to the estimate of ρ_c as 1.436 325 05(5). Thus we set our final estimate as $\rho_c = 1.436 325 05(10)$, where the error bar is quoted as twice the statistical error to account for possible systematic errors. The systematic errors may be due to higher-order scaling terms or the very small finite-size correction not included in the fits. Figure 11 shows a plot of P_B versus L at three different values of ρ that are very close to the critical point. It is found that the data points at $\rho_c \simeq 1.436 325 0$ distribute around $P_B = 0$ regardless of the system size L , i.e., the finite-size correction in P_B is undetectable at criticality. The obvious deviation from $P_B = 0$ when $\rho \neq \rho_c$ illustrates the reliability of our estimate of ρ_c .

For R_2 and R_0 , the value of O_0 is fixed at the theoretical predictions in the fitting. The data up to $L_{\min} = 16$ have to be discarded for a reasonable residual χ^2 . The results support the presence of the leading correction term $\sim L^{-2}$ with the amplitude $b_1 \simeq 0.12$. Together with the fact that the coefficient a_1 of R_2 and R_0 have the same amplitude but opposite signs, it is suggested that $R_2(\epsilon) = R_0(-\epsilon)$ with $\epsilon = (\rho_c - \rho)L^{y_1}$, which is expected from duality [52].

For Q , as seen from Fig. 10, the finite-size correction is much larger than that in R_2 and P_B . When the data are fitted to

Eq. (10), the coefficient b_2 has an error bar much larger than the central value. Thus fits are performed with fixed $b_2 = 0$. A large cutoff $L_{\min} = 64$ has to be set for a stable fit. The results show a leading correction term with exponent $y_1 \simeq -1.5$.

IV. DISCUSSION AND CONCLUSION

In summary, we study the critical polynomial P_B in nonplanar and continuum percolation models by MC simulations and FSS analysis. Two kinds of models are considered, i.e., the bond percolation model on square lattice with many equivalent neighbors (a nonplanar model) and the 2D continuum percolation of identical penetrable disks. As in planar-lattice models, it is found for these two models that $P_B = 0$ holds at

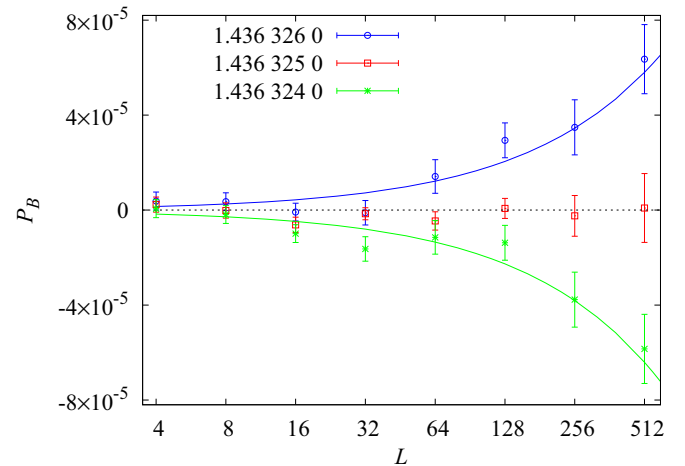


FIG. 11. Plot of P_B versus L at different mean densities ρ near criticality. Standard re-weighting technique is applied to obtain the data. Values of ρ are given in the legend. The curves are obtained by fitting the data.

the critical point as expected from universality, and that the finite-size correction in P_B is very small.

For P_B in the 2D equivalent-neighbor percolation model, from the data of the model with $z = 8$ neighbors, we find that the leading correction exponent is $y_1 \simeq -3$, much smaller than $y_1 \simeq -1.6$ for the wrapping probabilities and the ratio Q . For the latter quantities, the apparent leading correction term with $L^{y_1} = L^{-1.6}$ might be a mixture of L^{-2} , $L^{-2} \ln(L)$, and other irrelevant scaling terms [30]. For P_B , the value $y_1 \simeq -3$ is very close to $y_1 = y_t - \Delta_1 = -3.25$ for the first class of unsolved Archimedean lattices [25] mentioned in the introduction. The advantage of P_B over other quantities is more significant as z increases. Thus, for two types of equivalent-neighbor models with different ways to involve neighbors, P_B is employed to determine precisely the percolation threshold $p_c(z)$ for various values of z . The asymptotic behavior of zp_c is confirmed to be $zp_c - 1 \simeq a_1 z^{-1/2}$ for $z \rightarrow \infty$, with the coefficient a_1 being different for the two types of models. Since the regions of neighbors have different surfaces for the two types of models, the observed difference of a_1 could be regarded as evidence that the term $a_1 z^{-1/2}$ is a surface effect [35,36]. We also find that the subleading dependence of $zp_c - 1$ on z is proportional to z^{-1} .

Equivalent-neighbor percolation models have also been studied in more than two dimensions in the literature. For $d = 3$, while the implied surface effect suggests the $z \rightarrow \infty$ asymptotic behavior $zp_c - 1 \simeq a_1 z^{-2/3}$ [35,36], a most recent numerical study finds empirically $zp_c - 1 \simeq a_1 z^{-1/2}$ [40]. Since the maximum value of z considered in Ref. [40] is 146, it would be interesting to simulate systems with much larger z to clarify the ambiguity of the correction exponent. For $d \geq 4$, it is suggested that $zp_c - 1 \simeq a_1/z$ (with logarithm corrections in $d = 4$) [35,59], which implies that in this case the asymptotic behavior of zp_c is a bulk property. More work is needed to confirm the above asymptotic behavior for $d \geq 4$, and to understand the difference of the correction exponents in different dimensions.

For P_B in the 2D continuum percolation model, it is found that the finite-size correction is undetectable for $L \geq 3$. This implies that the leading correction exponent for P_B is much smaller than $y_1 \simeq -2$ and -1.5 for the wrapping probabilities and the ratio Q , respectively. Thus by using P_B , we are able to determine precisely the continuum percolation threshold as $\rho_c = 1.436\,325\,05(10)$. This estimate is slightly below the previous value $\rho_c = 1.436\,325\,45(8)$ obtained by analyzing the FSS of wrapping probabilities [34]. Our simulations are with smaller system sizes than the previous work as described in Sec. III A, but the resulting error bars of ρ_c are of the same order, i.e., 10^{-7} .

For unsolved planar-lattice percolation models at criticality, P_B usually has a very small leading correction term, such as $\sim L^{-3.25}$ or $\sim L^{-5.25}$ for unsolved Archimedean lattices [25]; and for exactly solvable lattice percolation problems, the finite-size correction in P_B vanishes for arbitrary size L . Might the continuum model be similar to the exactly solvable lattice models also for system sizes $L < 3$? To answer this, since L is not limited to integers, we perform additional simulations for system sizes $2 \leq L < 3$ at ρ_c . The result is shown in Fig. 12. A nonzero correction is observed for $L \leq 2.8$, which means that the finite-size correction in P_B does not vanish for arbitrary L ,

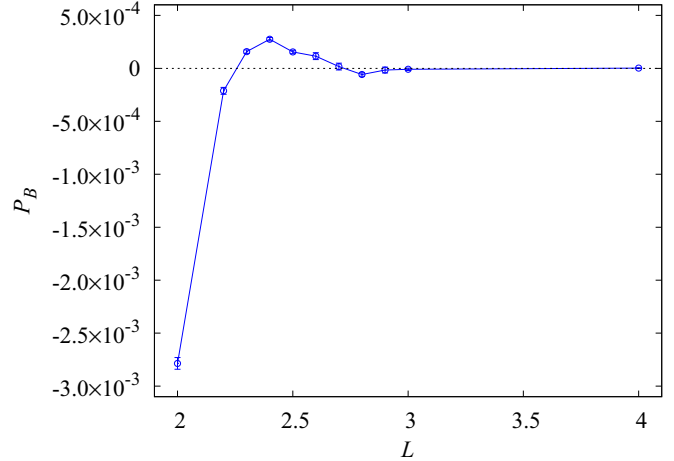


FIG. 12. Plot of P_B versus L for $L \leq 4$ in continuum percolation, at $\rho = 1.436\,325\,0$ that is within the error margin of the estimated critical point $\rho_c = 1.436\,325\,05(10)$. The line connecting data points is added for clarity.

although it is negligible for $L \geq 3$. It is nevertheless surprising to see that the amplitude of finite-size corrections is small and in order $O(10^{-3})$ even for $L = 2$.

Why the finite-size correction in P_B is so small in the 2D continuum percolation model remains an open question. For exactly solved lattice percolation models, the symmetry of the lattice can lead to the absence of correction terms in the FSS of P_B , which is proved by Mertens and Ziff [60] on self-dual lattices and self-matching lattices. Our results support that, in the continuum percolation model for $L \geq 3$, P_B is antisymmetric around p_c , which exactly holds for bond percolation on self-dual lattices [52].

The critical polynomial P_B can also be applied to study the continuum percolation of other shaped objects, the nonplanar Potts model in the FK representation, etc. P_B is currently defined in two dimensions. In more than two dimensions, one can also define various types of wrapping probabilities according to their topological properties. Is it possible to define a quantity similar to P_B from the combination of these wrapping probabilities? With the great success of the application of P_B in two dimensions, it is very attractive to explore the possibility. If found, then the quantity could have many applications, such as helping clarify the z dependence of $zp_c - 1$ for equivalent-neighbor percolation models with $d \geq 3$.

ACKNOWLEDGMENTS

We thank R. M. Ziff for very helpful comments. H.H. acknowledges the support by the National Natural Science Foundation of China (NSFC) under Grant No. 11905001 and by the Anhui Provincial Natural Science Foundation of China under Grant No. 1908085QA23. J.F.W. acknowledges the support by the NSFC under Grant No. 11405039. Y.D. acknowledges the support by the National Key R&D Program of China under Grant No. 2016YFA0301604 and by the NSFC under Grant No. 11625522.

- [1] D. Stauffer and A. Aharony, *Introduction to Percolation Theory* (Taylor & Francis, London, 1992).
- [2] S. R. Broadbent and J. M. Hammersley, *Proc. Camb. Phil. Soc.* **53**, 629 (1957).
- [3] P. N. Suding and R. M. Ziff, *Phys. Rev. E* **60**, 275 (1999).
- [4] M. F. Sykes and J. W. Essam, *J. Math. Phys.* **5**, 1117 (1964).
- [5] A. E. Kennelly, *Electr. World Eng.* **34**, 413 (1899).
- [6] L. Onsager, *Phys. Rev.* **65**, 117 (1944).
- [7] J. C. Wierman, *J. Phys. A: Math. Gen.* **17**, 1525 (1984).
- [8] C. R. Scullard, *Phys. Rev. E* **73**, 016107 (2006).
- [9] R. M. Ziff, *Phys. Rev. E* **73**, 016134 (2006).
- [10] R. M. Ziff and C. R. Scullard, *J. Phys. A: Math. Gen.* **39**, 15083 (2006).
- [11] J. C. Wierman and R. M. Ziff, *Electron. J. Combinatorics* **18**, P61 (2011).
- [12] R. M. Ziff, C. R. Scullard, J. C. Wierman, and M. R. A. Sedlock, *J. Phys. A: Math. Theor.* **45**, 494005 (2012).
- [13] F. Y. Wu, *J. Phys. C* **12**, L645 (1979).
- [14] G. R. Grimmett and I. Manolescu, *Probab. Theory Relat. Fields* **159**, 273 (2014).
- [15] R. Kenyon, in *Proceedings of the School and Conference on Probability Theory*, ICTP Lecture Notes Series, Vol. 17, LNS0417005 (ICTP Publications & Printing, Trieste, 2006).
- [16] C. R. Scullard and R. M. Ziff, *Phys. Rev. Lett.* **100**, 185701 (2008).
- [17] C. R. Scullard and R. M. Ziff, *J. Stat. Mech.*, P03021 (2010).
- [18] C. R. Scullard, *J. Stat. Mech.*, P09022 (2011).
- [19] C. R. Scullard, *Phys. Rev. E* **86**, 041131 (2012).
- [20] C. R. Scullard and J. L. Jacobsen, *J. Phys. A: Math. Theor.* **45**, 494004 (2012).
- [21] C. R. Scullard and J. L. Jacobsen, *J. Phys. A: Math. Theor.* **46**, 125006 (2013).
- [22] J. L. Jacobsen, *J. Phys. A: Math. Theor.* **47**, 135001 (2014).
- [23] J. L. Jacobsen, *J. Phys. A: Math. Theor.* **48**, 454003 (2015).
- [24] C. R. Scullard and J. L. Jacobsen, *J. Phys. A: Math. Theor.* **49**, 125003 (2016).
- [25] C. R. Scullard and J. L. Jacobsen, *Phys. Rev. Res.* **2**, 012050(R) (2020).
- [26] R. P. Langlands, C. Pichet, P. Pouliot, and Y. Saint-Aubin, *J. Stat. Phys.* **67**, 553 (1992).
- [27] H. T. Pinson, *J. Stat. Phys.* **75**, 1167 (1994).
- [28] L. P. Arguin, *J. Stat. Phys.* **109**, 301 (2002).
- [29] M. P. Nightingale in *Finite-size Scaling and Numerical Simulation of Statistical Systems*, edited by V. Privman (World Scientific, Singapore, 1990).
- [30] Y. Q. Ouyang, Y. J. Deng, and H. W. J. Blöte, *Phys. Rev. E* **98**, 062101 (2018).
- [31] B. Nienhuis, in *Phase Transitions and Critical Phenomena*, edited by C. Domb and J. L. Lebowitz (Academic Press, New York, 1987), Vol. 11. In Eq. (4.26) of this work, +1 should be change to +2.
- [32] K. Binder, *Z. Phys. B: Condens. Matter* **43**, 119 (1981).
- [33] Y. J. Deng, Y. Q. Ouyang, and H. W. J. Blöte, *J. Phys.: Conf. Ser.* **1163**, 012001 (2019).
- [34] S. Mertens and C. Moore, *Phys. Rev. E* **86**, 061109 (2012) This work uses an adaption of the Newman-Ziff algorithm: The simulation is conducted in the microcanonical ensemble where one disk is added at a time to the system. The wrapping probability is calculated as a function of the number of disks, which is convoluted with the Poisson distribution to give the grand-canonical wrapping probability as a function of the mean disk density ρ .
- [35] S. Frei and E. Perkins, *Electron. J. Probab.* **21**, 1 (2016).
- [36] S. Lalley, E. A. Perkins, and X. Zheng, *Ann. Probab.* **42**, 237 (2014).
- [37] N. W. Dalton, C. Domb, and M. F. Sykes, *Proc. Phys. Soc.* **83**, 496 (1964).
- [38] C. Domb and N. W. Dalton, *Proc. Phys. Soc.* **89**, 859 (1966).
- [39] N. W. Dalton and C. Domb, *Proc. Phys. Soc.* **89**, 873 (1966).
- [40] Z. P. Xun and R. M. Ziff, *Phys. Rev. E* **102**, 012102 (2020).
- [41] Z. P. Xun and R. M. Ziff, *Phys. Rev. Res.* **2**, 013067 (2020).
- [42] M. Majewski and K. Malarz, *Acta Phys. Pol. B* **38**, 2191 (2007).
- [43] Z. Koza, G. Kondrat, and K. Suszczynski, *J. Stat. Mech.* (2014) P11005.
- [44] K. Malarz, *Chaos* **30**, 123123 (2020).
- [45] Z. Xun, D. Hao, and R. M. Ziff, *Phys. Rev. E* **103**, 022126 (2021).
- [46] K. Malarz, *Phys. Rev. E* **91**, 043301 (2015).
- [47] M. Kotwica, P. Gronek, and K. Malarz, *Int. J. Mod. Phys. C* **30**, 1950055 (2019).
- [48] E. Luijten and H. W. J. Blöte, *Int. J. Mod. Phys. C* **6**, 359 (1995).
- [49] J. Machta, Y. S. Choi, A. Lucke, T. Schweizer, and L. M. Chayes, *Phys. Rev. E* **54**, 1332 (1996).
- [50] M. E. J. Newman and R. M. Ziff, *Phys. Rev. E* **64**, 016706 (2001).
- [51] Some recent work studying dimensionless ratios including: A. Malakis, N. G. Fytas, and G. Gülpinar, *Phys. Rev. E* **89**, 042103 (2014); H. Hu and Y. J. Deng, *Nucl. Phys. B* **898**, 157 (2015); J. T. Siebert, F. Dittrich, F. Schmid, K. Binder, T. Speck, and P. Virnau, *Phys. Rev. E* **98**, 030601(R) (2018); A. Azizi and M. Pleimling, *ibid.* **102**, 022112 (2020).
- [52] For bond percolation on self-dual lattices, due to duality, when the occupation probability p deviates from p_c by a small value satisfying $(p - p_c)L^y = \epsilon$, one has $R_0(-\epsilon) = R_2(\epsilon)$ and $R_0(\epsilon) = R_2(-\epsilon)$. Thus it can be proved that $P_B(-\epsilon) = -P_B(\epsilon)$, i.e., P_B is antisymmetric around $\epsilon = 0(p = p_c)$. This leads to the absence of scaling terms of the form $[(p - p_c)L^y]^n$ with even n for P_B . Due to universality, one expects that these properties are general in the FSS of the wrapping probabilities and P_B . This kind of analysis was performed for the spanning probability in J. P. Hovi and A. Aharony, *Phys. Rev. E* **53**, 235 (1996).
- [53] H. Hu, H. W. Blöte, and Y. J. Deng, *J. Phys. A: Math. Theor.* **45**, 494006 (2012).
- [54] J. Schmelzer, S. A. Brown, A. Wurl, M. Hyslop, and R. J. Blaikie, *Phys. Rev. Lett.* **88**, 226802 (2002).
- [55] E. T. Gawłinski and H. E. Stanley, *J. Phys. A* **14**, L291 (1981).
- [56] T. Vicsek and J. Kertesz, *J. Phys. A* **14**, L31 (1981).
- [57] A. Geiger and H. E. Stanley, *Phys. Rev. Lett.* **49**, 1895 (1982).
- [58] D. Frenkel and B. Smit, *Understanding Molecular Simulation: From Algorithms to Applications* (Academic Press, San Diego, CA, 2001).
- [59] R. van der Hofstad and A. Sakai, *Probab. Theory Relat. Fields* **132**, 438 (2005).
- [60] S. Mertens and R. M. Ziff, *Phys. Rev. E* **94**, 062152 (2016).